# Ag-Functionalized Carbon Molecular-Sieve Membranes Based on Polyelectrolyte/Polyimide Blend Precursors

By *Jonathan N. Barsema*, *Nico F. A. van der Vegt*, *Geert Henk Koops*,* and *Matthias Wessling*

We prepared dense flat-sheet Ag-functionalized carbon molecular-sieve (CMS) membranes from blends of P84 co-polyimide and a sulfonated poly(ether ether ketone) with a $Ag^+$ counterion (AgSPEEK). These blends offer the possibility of producing new functionalized precursor structures, which were previously not possible, such as integrally skinned asymmetric hollow fibers. Membranes prepared at a pyrolysis end temperature of 800 °C showed a maximum permeability for all tested gases at a Ag content of approximately 2.5 wt.-% (He permeability $P_{He} = 465$ Barrer (1 Barrer $= 7.5 \times 10^{-18}$ $m^2 s^{-1} Pa^{-1}$), $P_{CO_2} = 366$ Barrer, $P_{O_2} = 91.8$ Barrer, $P_{N_2} = 10.3$ Barrer). The maximum achieved selectivity for $O_2$ over $N_2$ with CMS membranes based on these blends was $\alpha_{O_2/N_2} = 13.5$ (Ag content: 4.5 wt.-%, $P_{O_2} = 52.7$ Barrer). The $CO_2$ over $N_2$ selectivity reached a value of 48.9 (Ag content: 4.5 wt.-%, $P_{CO_2} = 191$ Barrer). These observations are explained by the formation of selective bypasses around Ag nanoclusters in the CMS matrix.

## 1. Introduction

Recently, Koros and Mahajan[1] stressed the need for the development of new materials for gas-separation membranes, proposing the use of new mixed-matrix materials. These mixed-matrix materials allow for preservation of selectivity while showing significantly increased permeabilities. With these materials, one can break through the generally observed trade-off of selectivity versus productivity.[2] Well-known examples of these mixed-matrix materials are polymers with incorporated zeolite or carbon molecular-sieve (CMS) particles.[3–5] A new development is the preparation of mixed-matrix materials using nanosized particles. Merkel et al.[6] showed that the dispersion of nanosized nonporous silica particles significantly improved the membrane performance, with their only function being the increase of free volume at the silica–polymer interface. Barsema et al.[7] found that the incorporation of nanosized Ag particles into a CMS matrix resulted in an selectivity increase of $O_2$ over $N_2$ by 60 % while substantially increasing the permeability compared to the Ag-free CMS membrane. If one considers that CMS membranes have been reported with $O_2/N_2$ selectivity values over 30,[8,9] the potential of Ag-nanocluster-containing CMS (AgCMS) membranes is vast. Until now, AgCMS membranes have been prepared as flat-sheet, dense membranes. The presence of water-soluble $AgNO_3$ in the precursor composition restricts the range of possible precursor morphologies. In fact, one desires to produce, in a single step, an asymmetric structure with a dense gas-separation top layer and a non-selective mechanical-support layer. Generally, such a structure is prepared by phase inversion, where a non-solvent diffusing into a polymer solution induces de-mixing and phase separation. A polymer-poor phase forms the pores, and the polymer-rich phase forms the membrane structure.[10] Adding water-soluble Ag salts to the polymer solution is impossible, as the salt leaves the polymer matrix during phase separation. However, entrapping the $Ag^+$ ions through an ionic bond with a polymer may represent a concept for a state-of-the-art membrane-preparation method for an $Ag^+$-precursor membrane. In this article, we utilize polymeric blends containing $Ag^+$-loaded ion-exchange polymers, i.e., a sulfonated poly(-ether ether ketone) with $Ag^+$ as counterion (AgSPEEK).

## 2. Results and Discussion

### 2.1. Ag-Nanocluster-Containing Mixed-Matrix CMS Membranes

In a recent paper,[7] we reported the preparation of CMS membranes containing Ag nanoclusters for the separation of gases. By adding $AgNO_3$ to the doped solution of the precursor, we obtained a mixed-matrix membrane consisting of small (50 nm) Ag nanoparticles embedded in a carbon molecular-sieve matrix. Figure 1 shows a scanning electron microscopy (SEM) image of the cross-section of such a membrane.

It was hypothesized that these mixed-matrix CMS membranes can outperform their CMS counterparts in the separation of $O_2$ and $N_2$ through the creation of selective bypasses around the Ag nanoparticles. In these bypasses, which arise from the imperfect cohesion between the Ag and the carbon matrix, separation takes place based on the fast and selective mechanism of select surface flow. The interaction between $O_2$ and Ag allows the $O_2$ molecule to adsorb on the surface of the Ag particle and diffuse (either as a molecule or as dissociated single atoms) over the surface to desorb on the other side.

[*] Dr. G. H. Koops, Dr. J. N. Barsema, Prof. M. Wessling
Membrane Technology Group, Faculty of Science and Technology
University of Twente
P.O. Box 217, NL-7500 AE Enschede (The Netherlands)
E-mail: G.H.Koops@utwente.nl
Dr. N. F. A. van der Vegt
Max-Planck-Institute for Polymer Research
Ackermannweg 10, D-55128 Mainz (Germany)


DOI: 10.1002/adfm.200305155

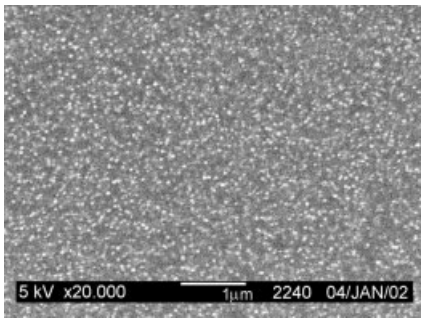


**Figure 1.** SEM image of the AgCMS membrane cross-section, using $AgNO_3$ as Ag source. (Pyrolysis end temperature was 700 °C, with 6 wt.-% $AgNO_3$ in polymer.)

A second effect of these bypasses is a significant increase in volume available for diffusion, seen in the increased permeability. This can be measured by determining the sorption capacity for gases (He, $N_2$, $O_2$, and $CO_2$) for both the CMS (coded as MP, followed by the pyrolysis end temperature) and a mixed-matrix–CMS (coded as MAg, followed by the pyrolysis end temperature) material, as shown in Figure 2a, where the dotted lines represent the CMS and the continuous lines represent the mixed-matrix–CMS materials. It is evident that the sorption increases significantly for all gases. However, the sorption selectivity of $O_2$ over $N_2$ does not increase significantly (< 5 %), indicating that the found increase in selectivity (60 %) is based on improved diffusion selectivity rather than on sorption selectivity. Remarkably, the He concentration in the carbon increases strongly with the addition of Ag nanoclusters, indicating the creation of new He-accessible volume. The total microporous volume available to $CO_2$ ($W_0$), as determined by the Dubinin–Astakhov plots (Fig. 2b), increased by more than 17 % from 0.23 $cm^3\,g^{-1}$ to 0.27 $cm^3\,g^{-1}$, providing an explanation for this large sorption increase.

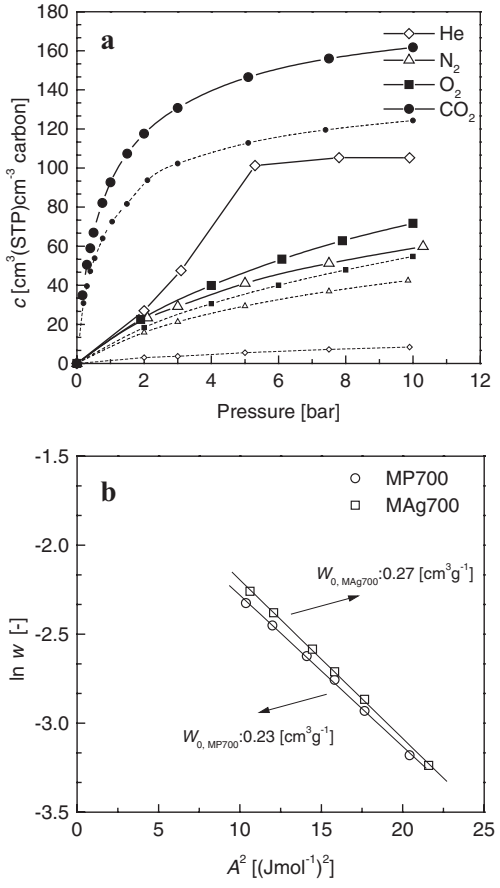


**Figure 2.** a) Gas concentration (He ◇, $N_2$ △, $O_2$ ■, and $CO_2$ ●) versus pressure for MAg700 (continuous line) and MP700 (dotted line). b) Dubinin–Astakhov plots for MP700 (○) and MAg700 (□) CMS membranes. $T = 25$ °C, where $W$ is the pore volume, $W_0$ is the total microporous volume available to the probe molecule, and $A$ is the sorption potential.

If our hypothesis of bypass formation is correct, the bypass has, in a two-dimensional view, two walls of different compositions. On one side, the wall is composed of Ag, and on the other side, of C; hence, one might also expect a permeability enhancement of carbon-interacting gas species, e.g., $CO_2$. Indeed, in Figure 3, which displays the selectivity of $CO_2$ over $N_2$, $O_2$ over $N_2$, and $CO_2$ over $O_2$, we see a substantial increase in the selectivity of $CO_2$ over $N_2$ with increasing pyrolysis temperature (and densification, leading to a decrease of bypass diameter), next to the known increase of $O_2$ over $N_2$ selectivity. Importantly, the selectivity of $CO_2$ over $O_2$ remains virtually unchanged, indicating that both molecules benefit equally from the bypass.

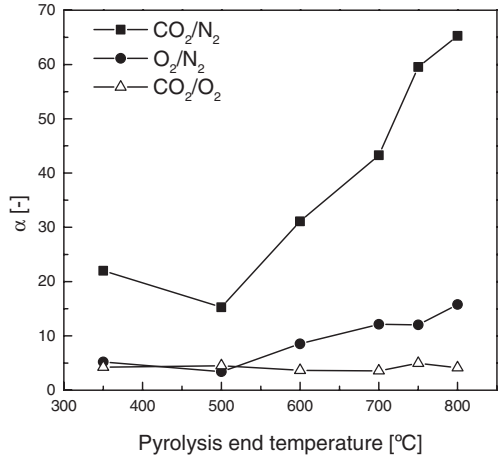


**Figure 3.** Selectivity of $CO_2$ over $N_2$ (■), $O_2$ over $N_2$ (●), and $CO_2$ over $O_2$ (△) versus the pyrolysis temperature for MAg membranes. Pressure $P = 2$ bar (1 bar = $1.0 \times 10^5$ Pa), $T = 25$ °C.

To extend the application of our material to industrial-gas separation, it is essential to prepare membranes with a high surface-to-volume ratio, combined with a high productivity. CMS membranes based on asymmetric hollow-fiber precursors with thin selective top layers satisfy these demands; however, they are generally prepared by phase-inversion spinning processes, using an aqueous non-solvent bath. Our precursor contains the highly water-soluble $AgNO_3$ as a Ag source, limiting the possibilities for precursor preparation. Therefore, we have chosen to develop a new concept for incorporating Ag nano-

  

ADVANCED FUNCTIONAL MATERIALS



clusters into the resulting CMS, by blending our precursor polymer with an Ag-containing polymer.

### 2.2. Blend Precursors for Mixed-Matrix AgCMS Membranes

Ag-containing polymers can be obtained by species-controlled ion exchange with ionomers. We use the well-known ionomer SPEEK, shown in Figure 4a, which is prepared by sulfonation of poly(ether ether ketone) (PEEK) and contains $SO_3^-$ groups that bind cations (e.g., $H^+$, $Na^+$, and $Ag^+$).

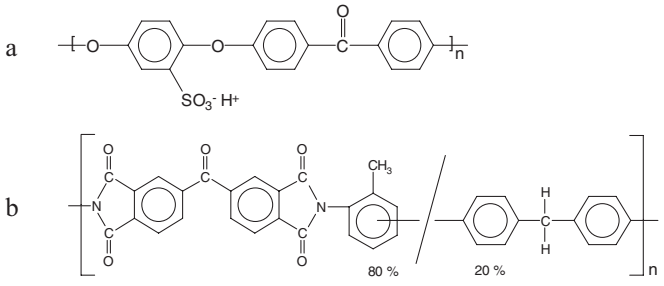


**Figure 4.** Chemical structures of a) SPEEK , b) P84 co-polyimide.

P84 co-polyimide (Fig. 4b) is a good precursor for CMS membranes.[7,11,12] By blending P84 co-polyimide with $Ag^+$-ion-exchanged SPEEK (AgSPEEK), one can obtain Ag-containing polymeric precursors for the preparation of CMS membranes. The AgSPEEK serves primarily as a Ag source, and the P84 forms the carbon matrix. Therefore, the pyrolysis behavior of the blend preferably should be close to that of P84. The prepared AgCMS membranes were coded MAgS, followed by the pyrolysis end temperature and AgSPEEK weight fraction (wt.-%), e.g., "MAgS700–10.0".

#### 2.2.1. Thermogravimetric Analysis

Thermogravimetric analysis (TGA) allows the pyrolysis progress to be followed closely, and reveals to what extent the blending alters the pyrolysis behavior of the major component. Figure 5 shows TGA curves for the pure components, as well as for three different blend compositions (5 wt.-%, 20 wt.-%, and 50 wt.-% AgSPEEK).

As the AgSPEEK content decreases, the pyrolysis behavior of the blends follows the behavior of P84 closely. The pure AgSPEEK shows a considerably different pyrolysis behavior as compared with P84. AgSPEEK shows a sharp increase in weight loss at temperatures just below 400 °C, then a plateau between 400 and 500 °C, and finally, a second weight-decrease step starting above 500 °C.

#### 2.2.2. Ion-Exchange Capacity of the Blend

The ion-exchange capacity (IEC) of the SPEEK was determined to be 1.61 meq $g^{-1}$. The counterion exchange can take place before or after blending with P84. The IEC of the blends

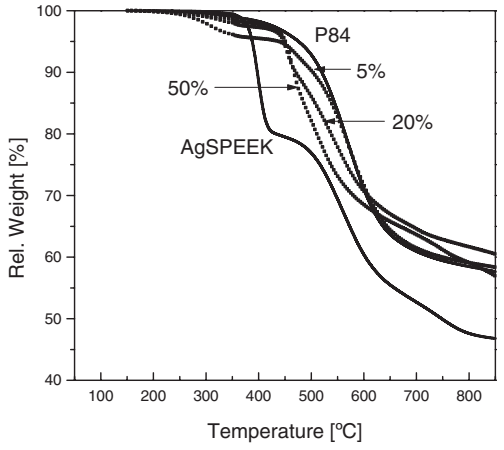


**Figure 5.** Relative weight decrease as function of temperature for various compositions of AgSPEEK/P84 blends measured by TGA.

was found to become less efficient as the SPEEK content was lowered (see Fig. 6). Therefore, we decided that blending prior to counterion exchange would lead to an inefficient use of the Ag-source capabilities of the SPEEK, and so we blended after $H^+$ was exchanged by $Ag^+$.

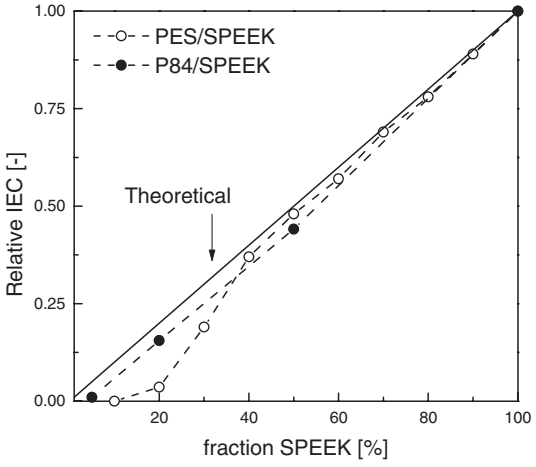


**Figure 6.** Relative IEC of poly(ether sulfone) (PES)/SPEEK [15] and P84/SPEEK blends versus the fraction SPEEK.

#### 2.2.3. Homogeneity of the Blend

To obtain a good distribution of Ag throughout the carbon matrix, it is essential to have a homogenous blend of P84 and AgSPEEK. This was verified using temperature-modulated DSC (tmDSC). Only one heating run could be conducted, as AgSPEEK can undergo chemical alterations due to the applied temperature, i.e., reduction of $Ag^+$ ions and thermochemical degradation.[13] Chun et al.[14] reported glass-transition temperatures ($T_g$s) between 195–210 °C for sulfonated PEEK with $H^+$ as a counterion (HSPEEK) prepared with different degrees of sulfonation. Figure 7 shows the heat flow (Fig. 7a) and com-

  

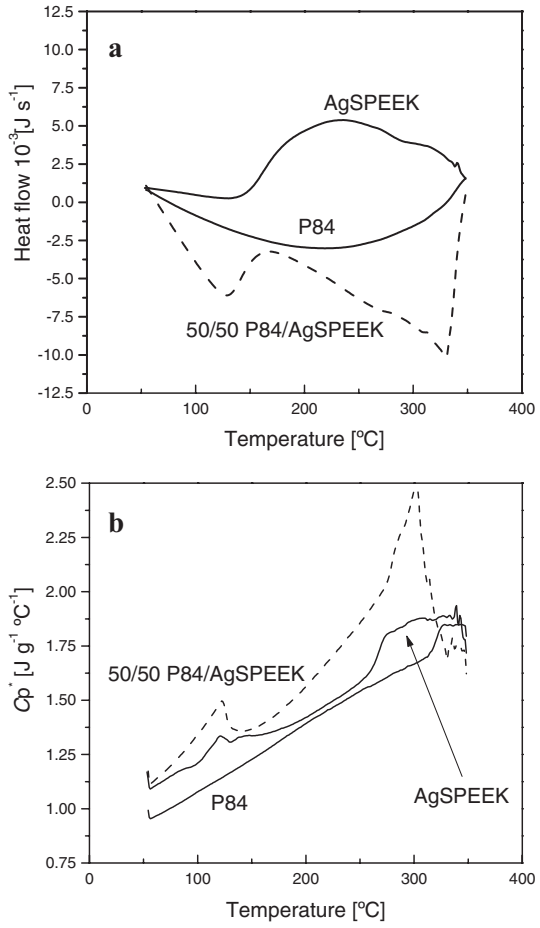


**Figure 7.** a) Heat flow and b) complex $C_p$ curves for P84, AgSPEEK, and a 50:50 blend of P84 and AgSPEEK obtained by tmDSC.

plex heat capacity $C_p$ (Fig. 7b) of P84, AgSPEEK, and an 50:50 blend of P84 and AgSPEEK, obtained by tmDSC. The reduction of $Ag^+$ to Ag is clearly visible in the heat-flow curves of both pure AgSPEEK and the blend, as a large increase in heat consumption is observed starting at approximately 125 °C. The blend curve shows a second temperature region with a high heat consumption beginning at 330 °C, which is also seen in the steep decrease of the $C_p$, indicating that a subsequent reaction is taking place. The $T_g$ of the investigated samples can be derived from the secondary transitions in Figure 7b. The values of $T_g$ for P84, AgSPEEK, and their 50:50 blend, as determined from the complex $C_p$ curves, are 317.2 °C, 266.3 °C, and 287.7 °C, respectively. The blended sample shows only one $T_g$, at a temperature of 287.7 °C, which is in good agreement with the theoretical value of 291.8 °C, obtained by applying the simple mixing rule. A second verification is obtained by plotting the measured IEC versus the fraction of SPEEK in the blend (Fig. 6). Figure 6 shows the relative IECs for two blends, poly(ether sulfone) (PES)/SPEEK[15] and P84/SPEEK, plotted versus the SPEEK fraction. Also, the theoretical IEC is added, obtained by applying a simple mixing rule. Wilhelm et al.[15] show that, for the inhomogeneous blend of PES and SPEEK, there is a threshold of 40 % SPEEK before the measured IEC of the PES/SPEEK approaches the theoretically predicted IEC. The threshold is explained by the formation of small, inaccessible de-mixed regions of SPEEK surrounded by a PES matrix. Compared to the PES/SPEEK blend, which shows the mentioned threshold, the P84/SPEEK blend approaches the theoretical IEC over the complete range of blend compositions. From these observations, we can conclude that, on a macroscopic level, the blend of P84 and AgSPEEK is homogeneous.

### 2.2.4. Sulfur Poisoning

A significant disadvantage of using an ionomer with sulfonic acid as a fixed ion is the presence of sulfur. It is well-known that sulfur acts as deactivator of Ag in catalysis systems,[16,17] as S readily covalently bonds with Ag. Oudar[17] states that a dissociation site for a $O_2$ molecule on Ag consists of two neighboring surface metal atoms, neither of which is bound to an adsorbed S atom. On either side of this pair of metal atoms, two vacancies must be located capable of receiving the dissociated O atoms. These vacancies cannot be in contact with a S-occupied site. This requires that a cluster of six adsorbate vacancies is available to dissociate one $O_2$ molecule. The presence of a small amount of sulfur atoms can thus influence the $O_2$ adsorption on Ag significantly. Although, according to the literature, the toxicity of the sulfur in $R–SO_3^-$ is reduced by a shielding effect of the surrounding oxygen atoms bonded to the central S atom,[16,18] it would be preferable to remove all S atoms during the pyrolysis. X-ray photoelectron spectroscopy (XPS) experiments on samples prepared at temperatures between 350–800 °C reveal the presence of Ag as well as S atoms on the surface of the membranes. It was attempted to perform XPS measurements on the cross section of the membranes. However, we were not able to obtain conclusive results, so we determined the composition of the bulk from the surface composition.

From the position of the XPS peaks, it is possible to determine the chemical nature of the Ag and S compounds, i.e., whether the sulfur is bound to silver, indicating the presence of both sulfur- and oxide-based Ag compounds.[19] The oxidation of Ag is caused by surface-to-air contact. We can therefore conclude that at all temperatures, part of the Ag is deactivated by S poisoning, and a reduced enhancement of the $O_2$ flux by the Ag must be expected.

### 2.2.5. Scanning Electron Microscopy

SEM images were taken from cross-sections of the MAgS800-5.0, MAgS800-9.1, and MAgS800-16.7 membranes. As an example, Figure 8 shows the cross-section of the MAgS800-16.7 membrane.

We could not identify large numbers of Ag nanoclusters, in contrast to the membranes prepared with $AgNO_3$, where the Ag clusters are found in abundance (see Fig. 1). We hypothesized that the formation of the Ag clusters starts with small clusters of $AgNO_3$, caused by an inhomogeneous distribution of the salt in the precursor. These clusters grow, after reduc-

  

ADVANCED FUNCTIONAL MATERIALS



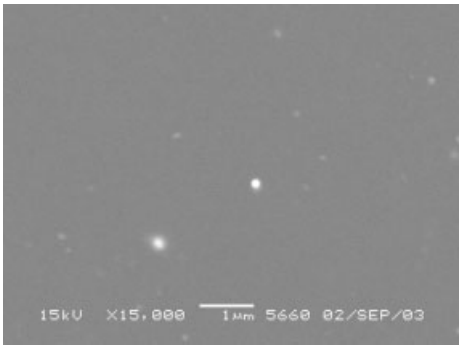


**Figure 8.** SEM image of the cross section of MAgS800-16.6.

tion, by Ostwald ripening,[20] sacrificing smaller clusters. In the blend precursors, the Ag atoms are uniformly distributed; therefore, only the process of Ostwald ripening is responsible for growth. These Ag clusters are too small to be observed (< 10 nm), or have not been formed at all, whereas the use of $AgNO_3$ as a Ag source results in clusters with sizes of 50 nm.[7]

### *2.2.6. Gas Permeation through AgCMS Membranes Based on P84/AgSPEEK Blends*

In Figure 9, we see the effect of Ag content in the CMS on the permeability of He, $CO_2$, $O_2$, and $N_2$. By adding different amounts of AgSPEEK to the precursor, indicated by the number, we varied the Ag content between 1 and 5 wt.-% of the carbon matrix (Table 1).

For comparison, the results[7] for a CMS membrane containing no Ag (MP800) and an AgCMS membrane based on a P84/$AgNO_3$ (MAg800) precursor were also added to Table 1. We must emphasize that, when adding up to almost 20 wt.-% of AgSPEEK, it is questionable whether one can speak of an additive and neglect the effect of the SPEEK on the carbonization process. A clear maximum permeability is reached at an Ag content of 2.46 wt.-%. Higher concentrations of Ag lead to the formation of Ag layers on the surface of the membranes, reducing the permeability and thereby counteracting the effect of the Ag clusters on the permeability.[7]

When plotting the selectivity of $CO_2$ over $N_2$, $O_2$ over $N_2$, and $CO_2$ over $O_2$ versus the Ag content (Fig. 10), we observe a trend comparable to that seen in Figure 3, where we could see an increase in selectivity for $CO_2$ over $N_2$ and for $O_2$ over $N_2$

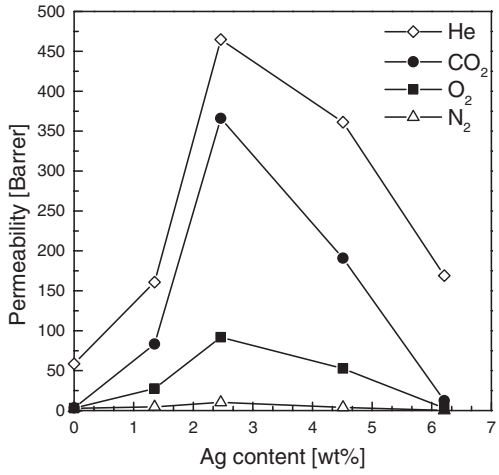


**Figure 9.** Permeability (1 Barrer = $7.5 \times 10^{-18}$ $m^2$ $s^{-1}$ $Pa^{-1}$) of He (◇), $CO_2$ (●), $O_2$ (■), and $N_2$ (△) versus Ag content. $P = 2$ bar, $T = 25$ °C.

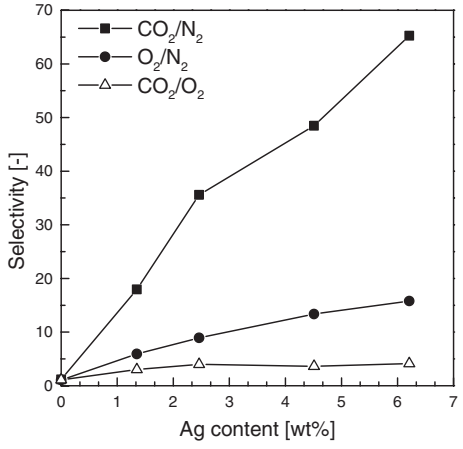


**Figure 10.** Selectivity of $CO_2$ over $N_2$ (■), $O_2$ over $N_2$ (●), and $CO_2$ over $O_2$ (△) versus the Ag content. $P = 2$ bar, $T = 25$ °C.

with increasing pyrolysis temperature. As shown in Figure 10, the same increase in $CO_2$ over $N_2$ and in $O_2$ over $N_2$ selectivity is observed with increasing Ag content. Again, the selectivity of $CO_2$ over $O_2$ remains virtually unchanged, indicating that the occurring changes have a comparable effect on the permeation of both molecules.

Where before, the increase of selectivity could be explained by a process of bypass formation and narrowing around Ag

**Table 1.** Effect of Ag content on permeation properties of He, $CO_2$, $O_2$, and $N_2$ for functionalized CMS membranes. $P = 2$ bar, $T = 25$ °C.

| Membrane | AgSPEEK content [wt.-%$_{in\ polymer}$] | Ag content [wt.-%$_{in\ CMS}$] | $P_{He}$ [Barrer] | $P_{CO2}$ [Barrer] | $P_{O2}$ [Barrer] | $P_{N2}$ [Barrer] |
|---|---|---|---|---|---|---|
| MP800 | 0 | 0 | 58.5 | 3.3 | 3.0 | 2.8 |
| MAgS800 | 5.0 | 1.35 | 161 | 83.3 | 27.5 | 4.6 |
| MAgS800 | 9.1 | 2.46 | 465 | 366 | 91.8 | 10.3 |
| MAgS800 | 16.7 | 4.51 | 361 | 191 | 52.7 | 3.9 |
| MAg800 | 6.0 [a] | 6.21 | 169 | 12.4 | 3.0 | 0.19 |

[a] $AgNO_3$ was used as Ag source instead of AgSPEEK.

  

nanoclusters, now the answer must be sought in the increasing number of bypasses created with increasing Ag content. As the number of bypasses increases, so does the number of regions where fast, favorable, surface diffusion of the adsorbed molecules takes place, resulting in a higher selectivity.

Although we expected a reduced functionality of our Ag present in the membrane because of S poisoning, this is not backed up by the experimental results. Hence, we overestimated the poisoning effect of S on the enhancement function of the Ag, or, quite possibly, the surface composition differs from the bulk composition.

Finally, Figure 11 shows the selectivity versus the productivity for the separation of $O_2$ and $N_2$. For reference, we have added the Robeson upper limit[2] that represents the trade-off between productivity and selectivity, observed generally for membranes. Depending on the required productivity and purity, one can now select the membrane with optimal performance.

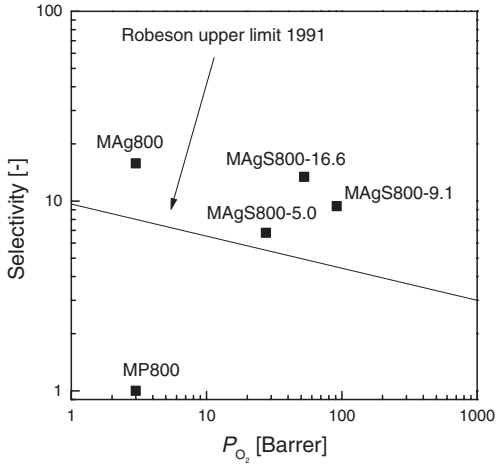


**Figure 11.** Selectivity of $O_2$ over $N_2$ versus the $O_2$ permeability for CMS membranes prepared at 800 °C with different Ag content. $P = 2$ bar, $T = 25$ °C.

## 3. Conclusions

By adding Ag nanoclusters to CMS membranes, we created mixed-matrix CMS membranes with improved selectivities for $O_2$ over $N_2$. From gas sorption measurements, we could determine that, for a membrane prepared at 700 °C, the total microporous volume available to $CO_2$ increases by 17 %.

We have shown that dense flat-sheet CMS membranes, prepared from blends containing P84 co-polyimide and Ag ion-exchanged SPEEK and pyrolyzed at 800 °C, have $O_2$ over $N_2$ separation properties exceeding the Robeson upper limit. By varying the ratio of P84 and AgSPEEK, the Ag content in the CMS membranes could be tailored, allowing us to find an optimal Ag content to maximize either permeability or selectivity. It was found that a maximum permeability was obtained for CMS membranes containing approximately 2.5 wt.-% of Ag ($P_{O_2} = 91.8$ Barrer, $\alpha_{O_2/N_2} = 8.9$), where the selectivity kept increasing as the Ag content increased (Ag content: 4.5 wt.-%, $P_{O_2} = 52.7$ Barrer, $\alpha_{O_2/N2} = 13.5$). An interesting side effect of the addition of Ag was the increase of the $CO_2$ over $N_2$ selectivity, reaching a value of 48.9 (Ag content: 4.5 wt.-%, $P_{CO_2} = 191$ Barrer). These observations were explained by the formation of selective bypasses around Ag nanoclusters in the CMS carbon matrix.

XPS analysis identified the presence of S compounds on the surface of the CMS prepared from a P84–AgSPEEK blend. Although it is well known that S can deactivate Ag catalyst, no negative effect on the gas separation performance of our membranes was found.

Using temperature modulated DSC and TGA analysis, we determined that our blend precursors are homogenous and have thermal properties close to that of P84.

These new blends provide the opportunity to prepare asymmetric structured precursors containing $Ag^+$ ions by phase inversion in aqueous non-solvents. Therefore, the production of mixed-matrix Ag-functionalized integrally skinned asymmetric CMS hollow fibers is within reach. This could not be obtained with previously proposed precursor composition and preparation methods.

## 4. Experimental

*Materials*: The blended-precursor membranes were prepared from the commercial, thermally stable, co-polyimide P84 (3,4,3′,4′-benzophenone tetracarboxylic dianhydride–toluene diisocyanate/methylene diphenyl isocyanate, BTDA–TDI/MDI) from Lenzing. The second blend component was sulfonated poly(ether ether ketone) (SPEEK). This polymer is obtained by sulfonation of poly(ether ether ketone) (PEEK). An extensive explanation of the preparation of SPEEK can be found elsewhere [15].

As a Ag source, $AgNO_3$ (Merck, 99.8 %), was used. *N*-Methyl-pyrrolidone (NMP, Merck, 99 %), was used as the solvent. All gases used for pyrolysis and gas permeation experiments had a purity of at least 99.5 %.

*Precursor Preparation*: Ion exchange, for both SPEEK and P84/SPEEK, was performed using the following protocol. The polymer was immersed in 1 M HCl for one day to obtain protonated SPEEK. Subsequently, it was rinsed with deionized water, followed by immersion in 4 M $AgNO_3$ for three days. During the last two steps, the solutions were renewed three times.

For the characterization of the blends, films were prepared from a solution of 13 wt.-% polymer in NMP. The solutions were allowed to dissolve overnight, and were subsequently filtered through a 25 μm metal filter.

The solutions were cast on glass plates using a 200 μm casting knife and placed in a $N_2$ dry box for three days. Finally, the films were placed in a $N_2$ oven for a further three days at 50 °C to remove most of the solvent. The relatively low temperature during the removal of the solvent was chosen to prevent premature reduction of the $Ag^+$ ions [7]. The obtained precursor film had a thickness of approximately 20 μm.

*Pyrolysis Procedure*: The pyrolysis was preformed using a Carbolite TZF 12/100 high-temperature tube furnace, mounted with a Eurotherm 2408 CP temperature controller. The precursor is placed in a quartz-glass tube, using a stainless-steel grid as a sledge. The atmosphere in the quartz tube during pyrolysis was $N_2$, with a flow rate of 10 $cm^3\,min^{-1}$.

A pyrolysis trajectory consisting of three steps was used for the preparation of the CMS and AgCMS membranes. In the first step, the precursor was heated to 150 °C (50 °C $min^{-1}$), and kept at this temperature for 15 min to remove adsorbed water. Subsequently, the temperature

  

was raised with a heating rate of 5 °C min$^{-1}$ to 350 °C, after which the pyrolysis end temperature was reached with a heating rate of 1 °C min$^{-1}$. Upon reaching the end temperature, the membranes were immediately quenched into $N_2$ to room temperature in an external stainless-steel double-hulled cooler. The membranes were cooled by flowing tap water through the outer hull of the cooler.

*Ion-Exchange Capacity*: The ion-exchange capacity of the prepared blends was determined by indirect titration with 0.1 N NaOH. The samples, approximately 0.7 g, were protonated by immersion in 250 mL of 1 M HCl for one day. The excess HCl was subsequently removed from the sample by rinsing for three hours using 250 mL of de-ionized water. The rinsing fluid was renewed three times, or until no $H^+$ could be detected in the wastewater using $AgNO_3$ as an indicator.

The protonated polymer was immersed in 50 mL 2 M NaCl or 4 M $AgNO_3$ solution, depending on the desired counterion ($Na^+$ or $Ag^+$). The immersion fluid was replaced three times, whereby the immersion fluid was collected for $H^+$ analysis by titration. In the case of $Ag^+$ exchange, an equal volume of 4 M NaCl was added to the retained immersion fluid to precipitate the remaining $Ag^+$ (as this will react with the $OH^-$ of the titration solution) and was removed by filtration. Subsequently, the total amount of released $H^+$ was determined by titration with 0.1 M NaOH. From the obtained proton concentration, we can determine the degree of sulfonation (*SD*) and the ion-exchange capacity (IEC) of pure SPEEK as well as of the blend by

$$IEC = \frac{SD \times 10^3}{x \times (M_{\mathrm{nSPEEK}} \times SD + M_{\mathrm{PEEK}} \times (1-DS)) + (1-x) \times M_{\mathrm{P84}}} \quad (1)$$

where *IEC* is the ion-exchange capacity in meq g$^{-1}$, *SD* is the degree of sulfonation, $M_R$ is the molecular weight of the blend component (where R is the type of component, SPEEK, PEEK, or P84; and n represents the counterion, $H^+$, $Na^+$, or $Ag^+$), and $x$ is the SPEEK fraction in the blend.

*Weight Loss*: The weight loss during heat treatment was determined using thermal gravimetric analysis (TGA). The TGA experiments were preformed using a Perkin-Elmer TGA 7 with a $N_2$ atmosphere and flow rates of 20 cm$^3$ min$^{-1}$. Heating routes were based on pyrolysis procedures described elsewhere [7].

*Differential Scanning Calorimetry*. Using differential scanning calorimetry (DSC), we could determine the glass-transition temperature $T_g$ and, therefore, the (in-)homogeneity of the prepared blends. For the DSC experiments, a Perkin-Elmer Pyris 1 DSC was used. Because the SPEEK thermally degrades at relatively low temperatures, only one heating run could be applied to the sample. Therefore, we choose to use the temperature-modulated DSC option provided by the Perkin-Elmer software (heating rate 2 °C min$^{-1}$, modulation amplitude 4 °C, period 60 s).

*Chemical Composition*: To investigate the presence and chemical nature of Ag and S, X-ray photoelectron spectroscopy (XPS) was performed using a Quantum 2000 Scanning ESCA Microprobe (Physical Electronics) on samples at different stages in the pyrolysis. The experiments were carried out on the surfaces of the samples, despite the occurrence of some oxidation evoked by contact with air [21].

*Scanning Electron Microscopy*: To investigate the distribution of Ag and Ag nanoclusters in the AgCMS structure, scanning electron microscopy (SEM) was used to look at both the cross sections and surfaces of the membranes. The micrographs were obtained using a JEOL JSM 5600 LV SEM.

*Gas Sorption*: The adsorption of gases in the carbon samples was determined using a Rubotherm magnetic-suspension balance operated by MessPro software. This balance has an accuracy of 1 μg and a reproducibility of 2 μg. The samples were evacuated to a pressure below 10 Pa before the gas pressure was applied. The obtained data were corrected for buoyancy effects, experienced because of the increased gas density at higher pressures.

Using the Dubinin–Astakhov equation and the sorption isotherm at low equilibrium pressures [22], the total microporous volume (for a certain probe molecule) can be determined. The Dubinin–Astakhov equation relates the pore volume $W$ to the sorption potential $A$,

$$W = W_0 e^{-\left(\frac{A}{E}\right)^n} \quad (2)$$

where $W$ is the pore volume, $W_0$ is the total microporous volume available to the probe molecule, $E$ is the characteristic energy of sorption, $n$ is equal to 2 [23], and $A$ is the sorption potential given by

$$A = RT \ln\left(\frac{p_s}{p}\right) \quad (3)$$

where $p_s$ is the saturation pressure and $p$ is the equilibrium pressure. The total microporous volume accessible to the probe gas can be determined from the $y$-axis intercept in a plot of ln $W$ versus $A^2$.

Received: November 28, 2003
Final version: June 28, 2004

[1] W. J. Koros, R. Mahajan, *J. Membr. Sci.* **2000**, *175*, 181.
[2] L. M. Robeson, *J. Membr. Sci.* **1991**, *62*, 165.
[3] D. Q. Vu, W. J. Koros, S. J. Miller, *J. Membr. Sci.* **2003**, *211*, 311.
[4] D. Q. Vu, W. J. Koros, S. J. Miller, *J. Membr. Sci.* **2003**, *211*, 335.
[5] J.-M. Duval, B. Folkers, M. H. V. Mulder, G. Desgrandchamps, C. A. Smolders, *J. Membr. Sci.* **1993**, *80*, 189.
[6] T. C. Merkel, B. D. Freeman, R. J. Spontak, Z. He, I. Pinnau, P. Meakin, A. J. Hill, *Science* **2002**, *296*, 519.
[7] J. N. Barsema, J. Balster, V. Jordan, N. F. A. van der Vegt, M. Wessling, *J. Membr. Sci.* **2003**, *219*, 47.
[8] M. B. Shiflett, H. C. Foley, *Science* **1999**, *285*, 1902.
[9] H. Suda, K. Haraya, *J. Phys. Chem. B* **1997**, *101*, 3988.
[10] M. H. V. Mulder, *Basic Principles of Membrane Technology*, 2nd ed., Kluwer, Dordrecht, The Netherlands **1996**.
[11] J. N. Barsema, N. F. A. van der Vegt, G. H. Koops, M. Wessling, *J. Membr. Sci.* **2002**, *205*, 239.
[12] H. B. Park, S. Y. Nam, J. G. Jang, Y. M. Lee, *Korean Membr. J.* **2002**, *4*, 25.
[13] F. Wang, T. L. Chen, J. P. Xu, *Macromol. Rapid Commun.* **1998**, *19*, 135.
[14] Y. S. Chun, H. S. Kwon, W. N. Kim, H. G. Yoon, *J. Appl. Polym. Sci.* **2000**, *78*, 2488.
[15] F. G. Wilhelm, I. G. M. Punt, N. F. A. van der Vegt, H. Strathmann, M. Wessling, *J. Membr. Sci.* **2002**, *199*, 167.
[16] C. H. Bartholomew, *Appl. Catal., A* **2001**, *212*, 17.
[17] J. Oudar, *Catal. Rev. - Sci. Eng.* **1980**, *22*, 171.
[18] J. B. Butt, E. E. Petersen, *Activation, Deactivation, and Poisoning of Catalysts*, Academic, San Diego, CA **1988**.
[19] C. J. Powell, *NIST Standard Reference Database 20: X-ray Photoelectron Spectroscopy Database*, Version 3.4, National Institute of Standards and Technology, Gaithersburg, MD **2003**.
[20] A. Heilmann, *Polymer Films with Embedded Metal Nanoparticles*, Springer, Berlin, Germany **2003**.
[21] C. W. Jones, W. J. Koros, *Carbon* **1994**, *32*, 1419.
[22] M. M. Dubinin, *Chem. Rev.* **1960**, *60*, 235.
[23] J. Hayashi, M. Yamamoto, K. Kusakabe, S. Morooka, *Ind. Eng. Chem. Res.* **1995**, *34*, 4364.

  